Chapter 10
On the Fractal Pattern Phenomenology of Geological Fracture Signatures from a Scaling Law

I. Gioveli, A.J. Strieder, B.E.J. Bodmann, M.T. Vilhena, and A.S. Athayde

10.1 Introduction

Geologic fractures geometry and their connectivity are considered the main features when it comes to prospection of hydrocarbon reservoirs and also for the search of aquifers, since it is becoming increasingly important in the question of freshwater supply [OdEtAl99], [Be00], [PuEtAl01], [DaEtAl06]. Although there is a common consensus that fractures are commonly caused by stress–strain exceeding the admissible rock strength, it is save to say that there does not exist yet a quantitative and concise theory that relates fractures patterns to their origin by compression, or tension during genesis [Ha85], [RaHu87]. There exist mathematical model approaches such as the Mohr–Coulomb model, which is far from being a useful formulation in order to simulate fracture patterns similar to those found in rocky areas.

The complexity on the fracture pattern genesis as well as the dynamics of geological fracture pattern formation gives us the motivation to focus our attention on determining scaling laws, as a first step into a direction that shall reveal in the future the dynamics that leads to the observed fracture signature. In fact in this work we show that the fractal dimension of the geological fractures at different scales is a manifestation of a clean scaling law for the fracture directions.

I. Gioveli
Federal University of Fronteira Sul, Santo Ângelo, RS, Brazil
e-mail: izagio@gmail.com

A.J. Strieder (✉) • A.S. Athayde
Federal University of Pelotas, Pelotas, RS, Brazil
e-mail: adelirstrieder@uol.com.br; alexandre.athayde.ufpel@gmail.com

B.E.J. Bodmann • M.T. Vilhena
Federal University of Rio Grande do Sul, Porte Alegre, RS, Brazil
e-mail: bardo.bodmann@ufrgs.br; vilhena@mat.ufrgs.br

It is notable that the directional step length range fits with considerable accuracy and affine feature in the log-log plane of step length by number of fractures with grid line intersections (to be introduced in the next section), suggesting a self-affine mechanism for fracture genesis. Hence, the present discussion is an attempt to translate the affine property of fracture direction occurrence into a fractal-discrete scheme, which represents the interactions of the shear or stress field with the considerable complex set of boundary conditions, established by the geological profile at each observable scale.

Fractal geometry has been a useful guide for understanding many natural patterns since it seems to be a common optimization solution used by Nature. The scale invariant fracture pattern is one of the many examples found in the geological scenarios where a fractal geometry is verified. In fact, the fracture hierarchy is composed by successive generations of fractures in different directions resulting from the multiple ramification of their antecedent (similar to a Cantor set construction), which reflects somehow the influence of the stress field modification by the presence of fractures of a given scale. From generation to generation, lengths diminish suggesting an underlying fractal geometry, which we confirm by our fractal analysis presented in Sects. 10.3–10.4.

In its consecutive generations ($n = 0, 1, 2 \ldots$), the hierarchy begins with the largest fracture scale, which gives rise to successive fracture scale subdivisions. The total of generations is finite by the fact that the analysis underlying images are limited by their resolution (i.e., the granular structure of outcrops, aerial photographs, remote sensing images among others) [Tu97]. Motivated by the fractal architecture of the fracture hierarchy scheme, which exhibits geometrically approximate self-similarity [Hi89], [Tu97], the present discussion is dedicated to the question whether affine characteristics and self-similar structure imposed by observational findings permit some sort of "reverse engineering" which may in a future work lead to an fracture pattern description implemented in a fractal discrete scheme [At99], [Ba04], [Ba84], [CaEtAl94], [CaCh95], [CaChCo03], [MoBoVa02], [PrVM03]. Such a procedure could replace the usual continuous formalisms based on mathematical spectral analysis which is in general too complicated when complex boundary conditions are involved.

The use of the fractal dimension method for geological fracture patterns is not new in the literature, for instance, in [VoKr04] it was used to analyze the apparent fracture intensity with their spatial orientation. General aspects of fracture systems in geological media with scaling laws were considered in [BoEtAl01], where the principal concern focused on the spatial distribution of fractures, the fracture intensity, and their self-similar appearance in different scales (see also [LaEtAl02], [NSEtAl05], [OrMaLa06]). To the best of our knowledge the perspectives that arise from our present discussion are new, since they may be considered a first step towards an approach that in a long term may open pathways for a dynamical fracture pattern genesis simulation beyond the phenomenological implementation, presented in this work.

Our article presents a study of the fractal dimension for an anisotropic fracture system which is typical for a selected geological site (Sect. 10.2), more specifically, homogeneous structural areas in Central Brazil (see Fig. 10.1). The fractal
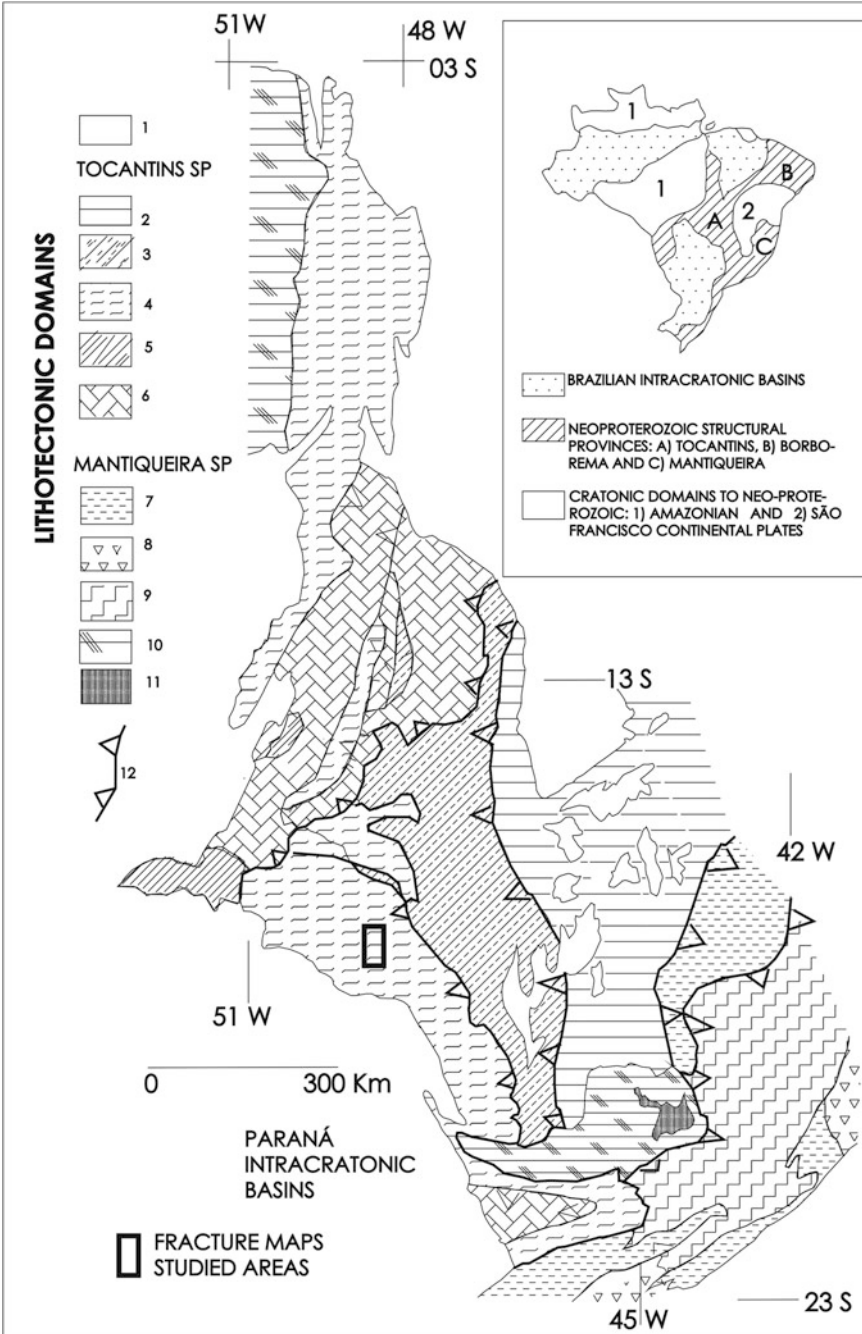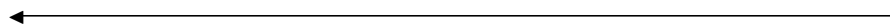
Fig. 10.1 (continued)

dimension was obtained by the Cantor Dust method [VeEtAl90], [VeEtAl91] for the fracture orientations which permits to establish the spatial fracture frequency distribution an essential input for the determination of the rock quality index as shown in [HuPr79].

10.2 Geological Setting of the Studied Areas

The studied areas are located in Central Brazil, in the Tocantins Structural Province (TSP, [AlEtAl81]). The TSP is a Neoproterozoic continental collision chain show predominantly north–south alignment. Of principal interest is the Abadiânia Nappe Thrust Sheet [StSu99], whose pseudo-stratigraphic $D1$ units are, from bottom to top: (a) Abadiânia Supersuite (Araxá metasedimentary suite and their Tectonic Block fragments suite), that correspond to an ophiolitic melange of the Neoproterozoic collision; and (b) a series of gneissifed units including Padre Souza Gneiss Suite, Maratá Lithodeme, Brumado Gneiss Suite, and others that are still being distinguished. The regional extent of the Abadiânia Nappe ($D2$ structure) from west to east developed a number of ESE tectonic inflexions, branching thrust faults and folds ($D3$ structures) in order to accommodate $D3$ deformation (see [StSu99] for details). The final deformation stage (retrogressive $D4$) corresponds to localized trans-current faults, controlled by a local stress field related to tectonic inflexions (see Fig. 10.2). One of the criteria for the choice of the area was good visibility of fractures over a considerable range of scales in order to analyze the fracture patterns for possible self-similarity [St93]. The Central Brazil (TSP) was not subject to younger deformational episodes, which is also the case for the areas located north, central, and south from the Serra do Fundão Inflexion. The fracture maps (shown in Fig. 10.2) for the Serra do Fundão in the scale 1 : 97000 were taken from [St93]. They originate from aerial photographs (1:110 000 scale) and printed LANDSAT TM5 images (221-072-X, band 5, scale 1:100 000; taken at the 16th of September of 1990; [St93]). Each fracture map represents the exact extension of the drainage linear segments, as observed in the aerial photographs and images.

Fig. 10.1 (continued) Geological setting of studied area in Central Brazil. (1) Phanerozoic sedimentary covers. Tocantins Structural Province; (2) undeformed low-grade meta-sediments; (3) Deformed low-grade meta-sediments; (4) Medium-grade meta-sediments (ophiolitic melange) and orthogneisses; (5) Neoproterozoic gneisses, granites, and volcano-sedimentary sequences; (6) Archean and Mesoproterozoic gneisses, granites, and volcano-sedimentary sequences. Mantiqueira Structural Province. (7) Deformed low-grade meta-sediments; (8) gneisses and granites of the Coastal Complex; (9) Granulytic gneisses of the Juiz de Fora Complex; (10) Cratonic granite-gneissic units of the (A) Amazonian and (B) São Francisco cratons. (11) Quadrilátero Ferrífero Greenstone Belt. (12) Main thrust faults
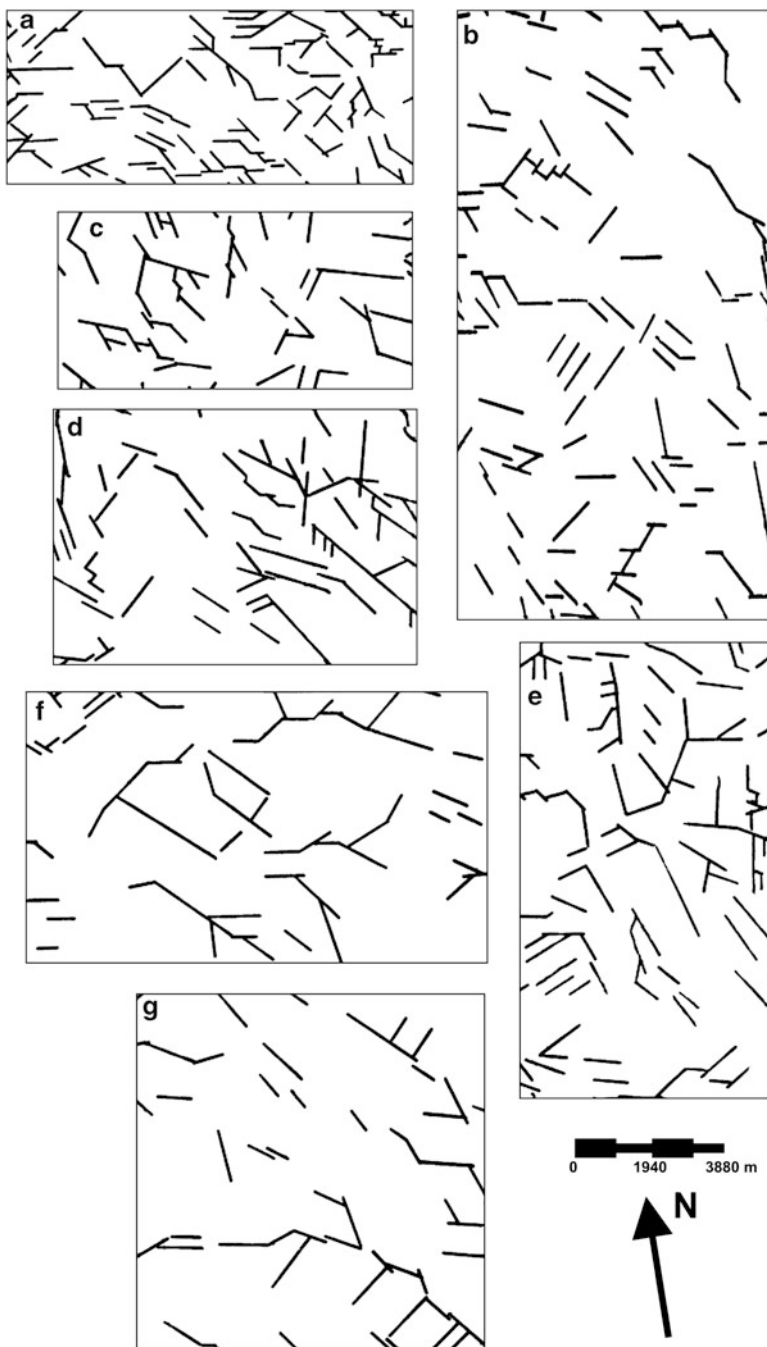
Fig. 10.2 Fracture maps in the Serra do Fundão region (GO, Brazil; scale 1:97 000), compiled from aerial photographs of reference Strider (1993). The maps are subdomains of the larger domain indicated by the box in the Fig. 10.1 and are located as arranged in the figure

## 10.3   The Fractal Dimension and Self-similarity Analysis

In order to perform the fractal dimension analysis we introduce in this section the adopted procedure, which if proven significant indicates the afore announced self-similarity. From the formal fractal construction point of view, a self-similar object with fractal dimension D may be divided into N smaller copies of itself scaled down by a factor r, where the number N is given in terms of the fractal dimension and the scaling factor by $N = \frac{1}{r^D}$. From the geometrical construction of the fractal the number of copies N and the ratio r are known, but the fractal dimension, that determines the scaling law, may be determined from the relation

$$D = -\frac{\log N}{\log r} \ .$$

Note that the construction of the fractal pattern with its self-similarity is not known a priori but shall be modeled in a progressive investigation, where the present fractal dimension analysis constitutes a first step. Already in [LiBZ05] it was pointed out that for natural objects the evidence for self-similarity may not be obtained by comparison of scales and simple counting of copies N per scale, in other words N and r, that are known in a theoretical construction of a fractal, are not directly accessible by observation, so that one has to resort to other techniques. For natural objects the dimensional Hausdorff–Besicovitch conception may be used, which may be implemented by a scaling law regression [GoMuMa98] from the box counting [Hi89], [Ba95] or the Cantor Dust method [VeEtAl90], [VeEtAl91], that yield the associated fractal dimension. It is noteworthy that each of these methods gives rise to a different fractal dimension for the same object [GiEtAl93], due to the fact that each method projects on a specific property that obeys a scaling law and in this sense they are complementary rather than contradictory. Since form observation the fracture orientation appears as a significant property in this paper the Cantor Dust method is used for the determination of the fractal dimension of the fracture maps. This dimension is a measure for the fracture density anisotropy concerning the trigonometric fracture orientation. For completeness we present in the following both methods and their resulting fractal dimensions.

The Cantor Dust method is applied on two-dimensional surfaces, i.e. the digitalized fracture maps of the Serra do Fundão region), following the reasoning of [VeEtAl90], [VeEtAl91]. To this end a C++ language program code was developed to automatically calculate $log(R)$ (length of steps) and $log(p)$ (ratio between total number of fractures per grid line intersections and total step number). The program code creates the orthogonal grid lines with varying step length (R) and trigonometric orientation to determine the fractal dimensions in different orientations. The Cantor Dust fractal dimension is then determined by the expression:

$$D = 1 - \frac{\log p}{\log R} \ . \tag{10.1}$$
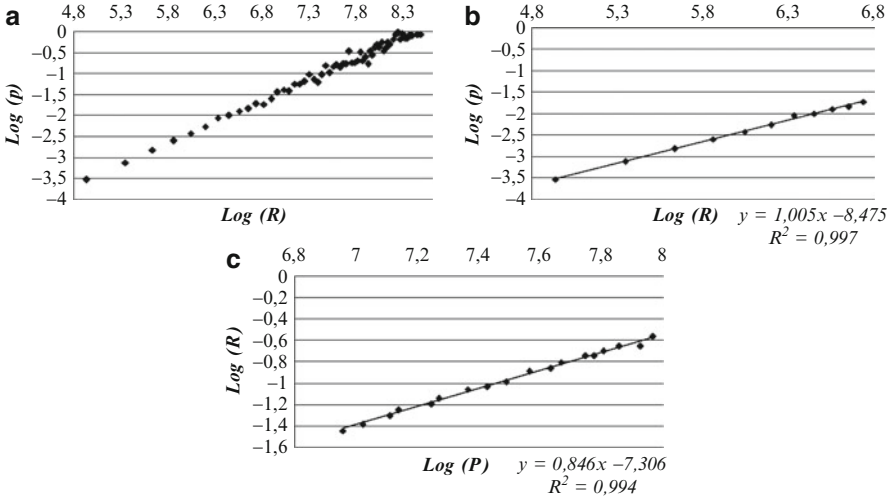
Fig. 10.3 The $log(p)$–$log(R)$ diagram and related fractal dimension by the Cantor Dust method. (**a**) Diagram for the whole range of p in a given area. (**b**) Diagram for the lowermost p values showing inclination close to unity. (**c**) Final diagram after eliminating lower and uppermost p values and showing the inclination of the linear correlation

The fractal dimension is determined from the linear correlation between $log(p)$–$log(R)$ (10.1) as shown in Fig. 10.3. In order to avoid errors in the fractal dimension due to physical limitations of the image (as granularity, for instance), lowermost p values are eliminated, when they show inclination close to unity (Fig. 10.3b); further p values larger than 0.8 are also eliminated when they show inclination close to 0 (for a detailed discussion of the cut application, see [VeEtAl91]). After application of the cuts the fractal dimension is obtained with a correlation coefficients larger than 0.97, which indicates a clear signature for a scaling law (see Fig. 10.3c).

As already announced before the Cantor Dust method is used in order to measure the anisotropy of the pattern, therefore the fracture maps are rotated sequentially by $10°$ counter-clockwise and for each orientation from 0 to $180°$ the fractal dimension is determined. A comparison between the respective orientations may be obtained using a polar plot, where for each angle the positive length $1 - D$ (i.e., the inclination of the regressions) is shown in Fig. 10.4. The anisotropy may be cast into two parameter form using the best fit with an ellipse for each fracture map by a procedure introduced in [HaFl98] and implemented with the *Matlab* program library. In the polar diagrams, the greatest and the smallest axis of the best fit ellipse indicates the directions of the higher and the lower inclinations of the $log(p)$–$log(R)$ diagrams. The measure for anisotropy is then defined by the axis ratio of the best fit ellipse. Thus, the larger the axial ratio, the larger the anisotropy of the fracture maps. Figure 10.5 shows the best fit ellipses for the set of fracture maps. Table 10.1 summarizes the found anisotropy parameters for each fracture map which may be related to the Serra do Fundão region in Fig. 10.2. According to our findings, the axis ratios range from 1.049 to 1.157.
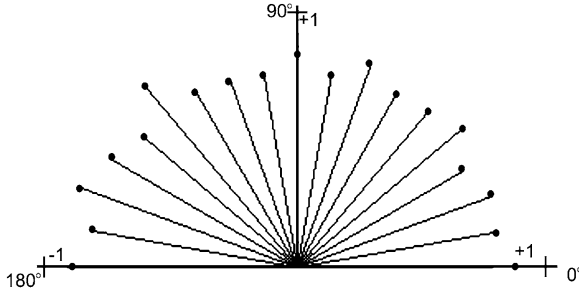
Fig. 10.4 Polar diagram of $1 - D$ for different grid orientations

The inclinations found in the $log(p)$–$log(R)$ plot from the Cantor Dust method show values in the range of 0.5 and 0.9 which corresponds to fractal dimensions between 0.5 and 0.1 for each trigonometric orientation and for each selected area. Figure 10.5 shows that the number of fractures intersecting with the reference grid is indeed anisotropic, where the ellipses of anisotropy show higher inclination if there is a larger number of fractures in other directions than the grid orientation; conversely it shows lower inclinations for a lower number of intersections. These directions are different for each fracture map area (see Fig. 10.2), where by inspection one observes differences in the preferred orientation for fractures in each area.

The second method mentioned above—the box counting method—is quite often used in order to analyze self-similarity. In the context of fracture patterns there exist applications in the literature, as, for instance, [Hi89], [AnEtAl98], [Ba95], [Ba01]. Note that by virtue box-counting captures the fracture length distribution but is not sensitive to the orientation of the pattern, which we believe to be the principal signature in the process of formation. A formal definition of the box-counting method may be found in [Fa97]. The basic procedure for the box-counting method makes use of a cover of the object by two- or three-dimensional boxes of edge length δ, where a total of N_δ boxes enclose the object completely. Upon rescaling the length to a fraction of the preceding one establishes a relation between δ and N_δ. In case of an apparent self-similarity the $log(\delta) - log(N_\delta)$ plot yields a scaling law, i.e., a linear correlation, a manifestation of a fractal dimension.

This definition is closely related to the question of the significance of the dimension determined by box-counting. The number of boxes (in the present case squares) of length δ that intersect the pattern is related to the dispersion or geometrical irregularity of the arrangement at the scale defined by δ. The numerical value of the fractal dimensions reflects the rapidity with which these irregularities evolve in the limit $\delta \to 0$. For practical applications there are limitations that have to be taken into account with respect to the maximum and minimum size of the boxes as exposed in detail in [GoMuMa98]. As an illustration we show this influence using the Koch curve as a test object with known fractal dimension $D = 1.2618$. The box-counting procedure was realized using the public domain
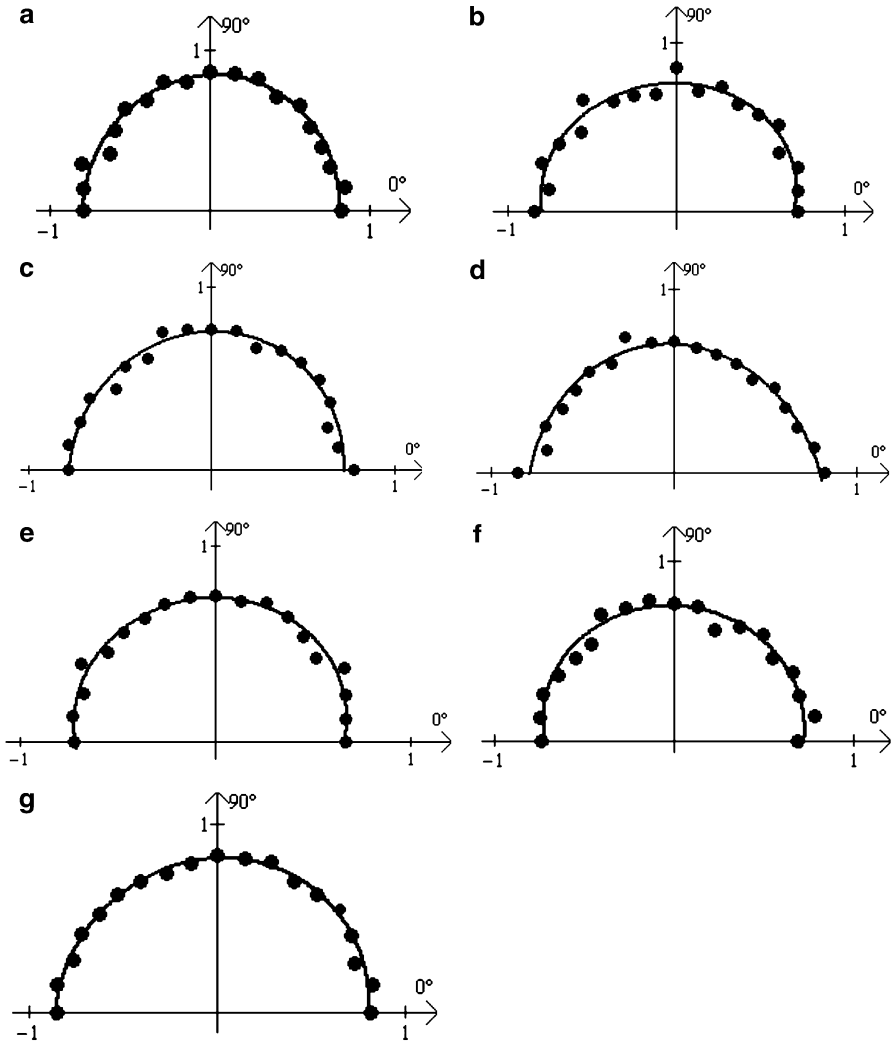
Fig. 10.5 Best fit ellipse polar plots of the fracture maps (scale 1:97 000) for the Serra do Fundão region (GO, Brazil). The values on the ellipses represent the inclination in the $log(p)$–$log(R)$ plot (**a**)–(**g**) for the respective fracture maps of the areas (**a**)–(**g**) in Fig. 10.2

software *FracAnalysis*. The fractal dimension and the box-counting method are related by the inclination

$$D = -\frac{\log N_\delta}{\log \delta} \,,$$

which is illustrated in Fig. 10.6 for different maximum and minimum sizes, as well as different scale changes.

Table 10.1 Best fit ellipse parameters for fracture maps (scale 1:97 000) for the
Serra do Fundão region (GO, Brazil)

Fracture map	Large axis direction	Small axis direction	Axis ratio	Ellipse origin
A	74°	164°	1.049	$(-0.008; 0.012)$
B	7°	97°	1.171	$(-0.067; 0.108)$
C	58°	148°	1.05	$(-0.002; -0.029)$
D	102°	12°	1.157	$(0.045; -0.236)$
E	7°	97°	1.117	$(-0.043; 0.1064)$
F	170°	80°	1.12	$(0.026; 0.098)$
G	43°	133°	1.06	$(0.01; 0.023)$
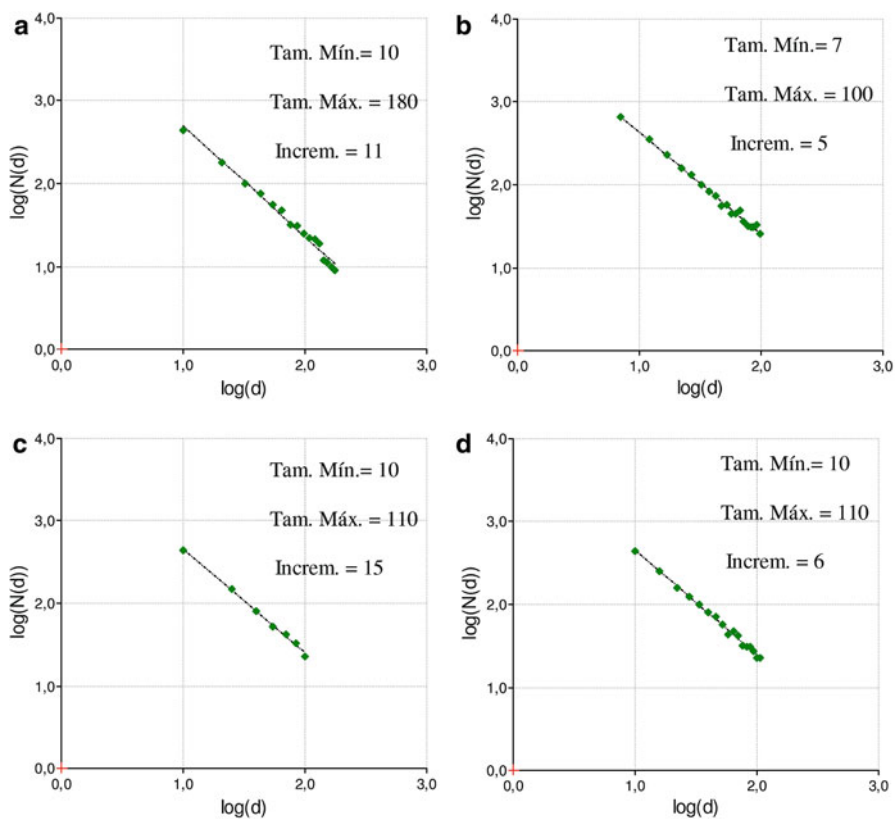
Fig. 10.6 Fractal dimension analysis of Koch's curve, for different box sizes and box rescaling.
The minimum and maximum box sizes and increments are (**a**) min = 10, max =180, incr = 11;
(**b**) min = 7, max = 100, incr = 5; (**c**) min = 10, max = 110, incr =15; (**d**) min = 10, max = 110,
incr = 6

Table 10.2 Fractal dimension of the fracture pattern maps (scale 1:97 000) of the Serra do Fundão, (Goias, Brazil)

| Map	A	B	C	D	E	F	G
Fractal dimension	1.3978	1.2608	1.2510	1.3443	1.3246	1.2450	1.1511
No. of fractures	134	128	65	77	108	59	53

The first two plots Fig. 10.6a, b are evaluated using 15 and 20 points, the non-adequateness of the maximum and minimum box sizes imposes a visible error. The third plot shows already a reasonable result for the fractal dimension, which is confirmed by the last plot where the number of box sizes was increased. The obtained result is in agreement with the theoretical expected value and also validates the program as a useful tool, once the minimum box size is not smaller than the smallest visible characteristic length of the curve, which analogously applies for the maximum box size in comparison with the largest observable characteristic length (see also [KuUmPa97]).

Application of the box-counting method to the thrusts in Japan yielded fractal dimensions between 1.05 and 1.60 [Hi89], the same method applied to fracture patterns observed in a copper mine in Arizona (USA) showed fractal dimensions between 1.34 and 1.92 [GhDa93]. Another work [Ba95] considered fracture patterns in the Yucca Mountain region (USA) and obtained numerical values between 1.12 and 1.16. The differences in the findings for the fractal dimensions are likely to be related to the different histories that caused the fracture patterns.

Further analyses are based on the digitalized fracture maps of the Serra do Fundão region (Goias, Brazil) and made use of the program *FracAanalysis*. The following procedure was adopted: The smallest admissible box size was chosen such as to be slightly larger than the smallest fracture size, whereas the largest box size was fixed in order to contain the whole pattern following the prescription in [Ba95]. The box size scaling was chosen in step/sizes such that the *log–log* plot contained between 15 and 20 points. The results for the box-counting method are shown in Table 10.2.

From the fact that the double logarithmic plots (Fig. 10.6) show a clear scaling law permits to interpret the scaling in Table 10.2 in terms of fractal dimensions that range between 1.1511 and 1.3978. Here the larger fractal dimension corresponds to the fracture map with a more dense and more complex structure, so that one may conclude that box-counting captures mainly fracture length density.

From our explanations concerning the two methods, Cantor Dust and box-counting, it becomes apparent that both methods are rather complementary and not contradictory, since they measure different properties of a specific map. As expected Cantor Dust is a method that indicates anisotropy which for a surface map has only an angular degree of freedom so that the fractal dimension shall be between 0 and 1, whereas the fractal dimensions by box-counting range from 1 to 2. Note that the same reasoning as in Cantor's Dust method was proposed by Buffon in 1777 to determine the numerical value of π but making use of non-isotropy of the method.
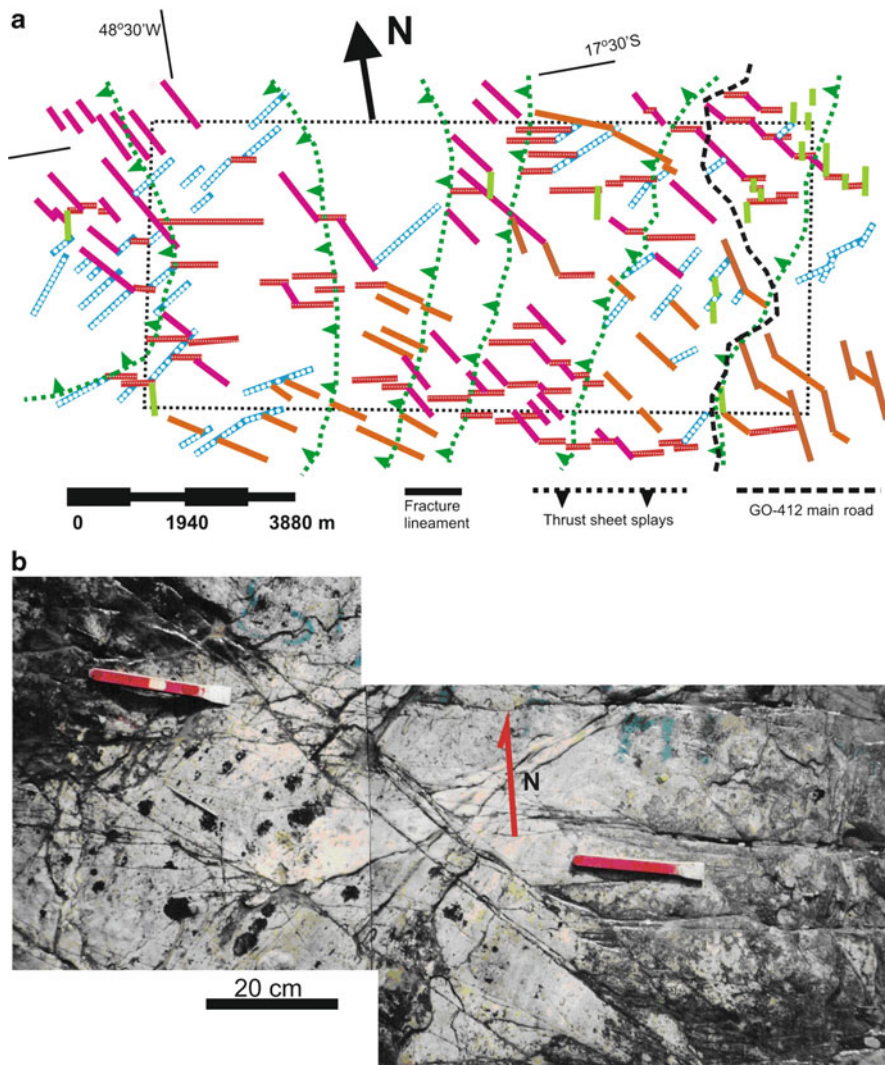
Fig. 10.7 Fracture maps for area A in the Serra do Fundão region (GO). (**a**) Fracture lineament map interpreted from satellite images and aerial photographs. (**b**) Outcrop scale fracture pattern in the selected area

Figure 10.7 shows a significant correlation of fracture alignments for certain areas, which indicates that for the further study the Cantor Dust analysis is the adequate tool for the fractal dimension analysis. Anisotropy is verified determining the inclination in the $\log(p)$–$\log(R)$ plots for a sequence of orientations as shown in the following sections.

10.4 Structural Fracture Analysis

In the last section scaling laws for fracture length density as well as anisotropy was verified using quantities that are related to the technique that allows to determine the fracture pattern associated fractal dimension. Moreover it is desirable to translate the procedure variables into those that refer directly to an observational quantity, the fracture frequency (f) and the respective length scale R (i.e., the step length). The fracture frequency (f) is a measure of the fracture quantity in a given rock mass, which depending on the consideration may be expressed in either of three ways: (a) the number of fractures per unit volume, (b) the number of fractures per unit area, and (c) the number of fractures per unit length in a given direction [TeEtAl05], where the latter is of interest for the remaining discussion.

Recalling that the linear fracture frequency can be defined by the ratio between the number of fractures that intersect a unit sample step of a given direction and the length R of this unit step, one may directly relate f, R, and p, where the latter is known to count the total number of fractures per grid line intersections and total step number (see (10.1)), so that $f = p/R$. The fractal dimension from (10.1) may be cast in to the form

$$D = -\frac{\log f}{\log R}.$$

For the purpose of simulating or constructing fracture patterns the scaling law that relates the fracture frequency and the length scale is then given by the inverse proportionality $f = R^{-D}$. An alternative interpretation of the linear fracture frequency is taking its inverse which is the fracture spacing in a given direction. The direct proportionality of fracture spacing and scaling is a manifestation of the aforementioned reasoning, that oriented fractures of one generation are the boundaries for the fractures of the subsequent scale a symmetry feature that a genuine dynamical equation for fracture pattern formation shall obey.

However, Fig. 10.5 and Table 10.1 show that fracture systems vary from one site to another in the Serra do Fundão region (GO). This anisotropic fracture distribution is due to the different fracture patterns present in each area. In fracture map for area A one identifies a strike slip duplex pattern, as can be seen in the map (Fig. 10.7a), and in the outcrop (Fig. 10.7b). The fracture lineaments map (Fig. 10.7a) can be seen as sets of straight lines, where each set may be parametrized by a linear equation $y = ax + b$, if one aligns the y-axis from south to north and the x-axis from west to east, which yields the fracture lineament in vector form $\lambda = (x, y)^T$ (see also [Pi56]). From the angular distribution, one recognizes six fracture families as shown in the rose diagram (Fig. 10.8). Each family may be characterized by an average fracture direction and a mean fracture length. The findings are given in Table 10.3.

From a comparison of Tables 10.1 and 10.4 one observes that the small axis direction for the best fit ellipse in fracture map A is close to the mean direction for fracture family 2 (Table 10.3). Fracture family 2 shows the highest fracture frequency or equivalently resulting in the lower intersection number for this direction. The highest inclination (highest f) in Fig. 10.5a is between 70 and 90°
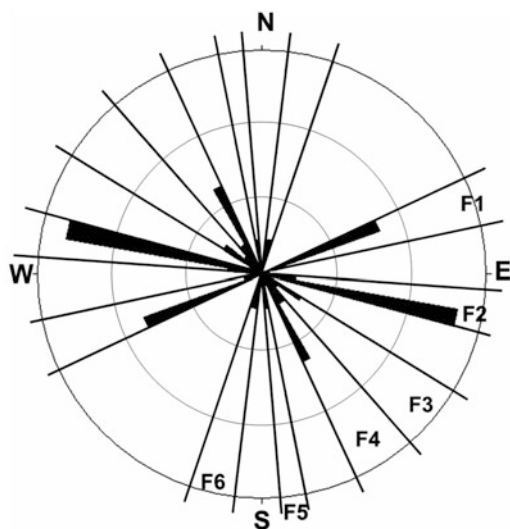
Fig. 10.8 Rose diagram for fracture lineaments in area A in the Serra do Fundão (GO) region. The outer circle represents 30% of the total (135) fracture lineaments in the map area

Table 10.3 Results for vector analysis of fracture lineaments in map A in the Serra do Fundão (GO) region. Fracture families are distinguished by the rose diagram. The geographic azimuth angles are transformed into trigonometric ones

|	Fracture family range in °	Number of fractures	Mean direction°	Mean length m	Mean direction dispersion	Mean length variation
Total	000–180	135	120.42	390.83	3.46	36.85
Family 1	010–025	27	021.38	749.19	0.68	59.22
Family 2	165–175	42	169.05	594.99	0.23	42.47
Family 3	135–160	18	145.46	977.05	2.17	105.99
Family 4	120–135	33	122.35	682.14	0.96	52.30
Family 5	095–100	6	098.78	792.12	0.28	115.26
Family 6	075–085	9	079.97	330.83	0.35	37.75

indicating the highest number of intersections. The classification into families may now be used for simulating a fracture pattern, as shown in the next section.

10.5 Fracture Lineament Map Simulation

The fracture lineament map is then simulated according to the fractal dimension and taking into account the identified fracture lineament families, represented by their respective line equation (Table 10.4). The mean direction and length and also their deviation is then used to define an angular coefficient (a) for each fracture

Table 10.4 Equations defining each fracture lineament family present in map A in the Serra do Fundão (GO) region. Variation coefficients are presented and defined according to Table 10.3, and n is a real number

	Fracture family range in °	Fracture lineament equation	Number of simulated fractures
Family 1	010–025	$y = (0.3914 \pm 0.011913)x \mp n7.0313$	24
Family 2	165–175	$y = \pm n1.9413$	38
Family 3	135–160	$y = (-0.6882 \pm 0.037977)x \mp n14.2278$	25
Family 4	120–135	$y = (-1.57848 \pm 0.016716)x \mp n28.9462$	20
Family 5	095–100	$y = (-6.477923 \pm 0.004911)x \mp n58.1902$	7
Family 6	075–085	$y = (5.652498 \pm 0.0061)x \mp n53.1228$	9
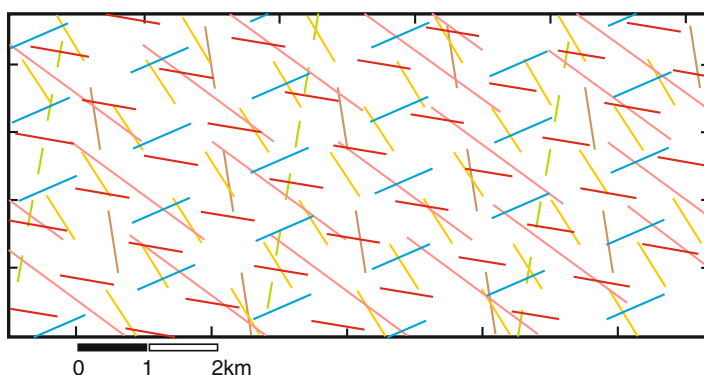
Fig. 10.9 Simulation of fracture map for area A in the Serra do Fundão region (GO, Brazil)

lineament family. Due to the finiteness of the lines it is sufficient to generate a specific position (x, y) for the whole set of lineaments of a specific family. Since such a simplification might cause that line segments overlap, such a coincidence may be reduced in the simulation making use of the constraint given by the fracture spacing $S = R^D$. Moreover, taking into account that lines of one family are parallel in the model simulation, b is related to fracture spacing by $b = R^D \sqrt{a^2 + 1}$. Thus, calculating b for each fracture family and replacing a and b in the linear equation yields the third column in Table 10.4.

The simulation was implemented in form of a *Matlab* code using the afore established rules. For each fracture family a representative was created to construct the lineament map as shown in Fig. 10.9.

10.6 Conclusion

In the present work we analyzed the fracture pattern in rocks for the Serra do Fundão region (GO, Brazil), which is the signature for the dynamics of rock evolution for that region. Our discussion showed that fractal analysis is beyond a mere

classification scheme but closely related to the dynamics by virtue of a clear self-similarity signature. We came to this conclusion by the structural geology analysis, where we distinguished different fracture sets that after parametrization was used to simulate a fracture lineaments map. These by inspection reproduced some characteristics of the original map, i.e. the fracture directional arrangement. The analytical fracture simulation took into account fracture direction and frequency, and the fractal dimension.

Those quantities are also relevant for rock qualification indexing that consider the fracture frequency in their computation. As was shown by the Cantor Dust approach, the fractal dimension can be related to the fracture frequency and fracture spacing commonly used in structural geology and rock mechanics. Cantor Dust is a one-dimensional embedding related to anisotropy (depending on the angle only) and thus the fractal dimension shall be $0 < D < 1$, whereas box-counting measures the length density distribution which implies in a fractal dimension $1 < D < 2$. From our explanation we showed that those different findings are a consequence of the procedure's complementary character, because each procedure captures a different aspect from the same phenomenon.

We are completely aware of the fact that our discussion is far from being complete. Nevertheless, the clear relation of the scaling law and the reasoning that fractures of larger scales play the role of boundaries in smaller scales and thus contemplates a more profound understanding of the fracture pattern signature. In this sense, a reproduction of our model theory could be implemented in laboratory, starting with a non-homogeneous and flat material sheet that is stretched beyond its admissible elastic limit and thus create a fracture pattern that should have a self-similar signature.

From the theoretical point of view we consider our contribution as a first step into a direction where the fracture dynamics may be understood in terms of some sort of inverse engineering, where the fractal scheme may substitute the otherwise necessary dynamical equation system with its constraints and boundary conditions in order to establish, which is known as a dynamical model. Such an approach may open pathways for a progressive modeling of fracture pattern pathology and in future hopefully for genesis of rock formation with its dependence on cooling and implications on shear stress fields. Although this may appear speculative, we at least believe to have shown with the present work that fracture analysis by self-similarity contains far more information than taxonomic ones, an impression that works known from the literature quite often transmit.

Of course it would be desirable to shed further light on some of the presented ideas that we postpone to a future work. An immediate challenge resulting from the presented discussion is the exploration of the self-similarity underlying scale invariance which we will cast into a simplified dynamical model for fracture pattern generation. In parallel, simulations will be improved implementing the combination of findings by the Cantor Dust and the box-counting method. Works in this direction may turn useful in the future once a more detailed comprehension of rock history will give further information for prospection site selections.

References

[AlEtAl81] Almeida, F.F.M., Hasui, Y., Neves, B.B.B., Fuck, R.A.: Brazilian structural provinces, an introduction. Earth Sci. Rev. **17**, 1–29 (1981)

[AnEtAl98] Angulo-Brown, F., Ramirez-Guzman, A.H., Yepez, E., Rudoif-Navarro, A., Pavi-amiller, C.G.: Fractal geometry and seismicity in the Mexican subduction zone. Geofísica Int. **37**, 29–33 (1998)

[At99] Atkins, A.G.: Scaling laws for elastoplastic fracture. Int. J. Fract. **95**, 51–65 (1999)

[Ba01] Babadagli, T.: Fractal analysis of 2-D fracture networks of geothermal reservoirs in south-western Turkey. J. Volcanol. Geoth. Res. **112**, 83–103 (2001)

[Ba95] Barton, C.C.: Fractal analysis of scaling and spatial clustering of fractures. In: Barton, C.C., La Pointe, P.R. (eds.) Fractals in the Earth Sciences, pp. 141–178. Plenum, New York (1995)

[Ba84] Bažant, Z.P.: Size effect in blunt fracture: concrete, rock, metal. J. Eng. Mech. **110**, 518–535 (1984)

[Ba04] Bažant, Z.P.: Scaling theory for quasi-brittle structural failure. PNAS **101**(37), 13400–13407 (2004)

[Be00] Berkowitz, B.: Scaling of fracture connectivity in geological formation. Geophys. Res. Lett. **27**, 2061–2064 (2000)

[BoEtAl01] Bonnet, E., Bour, O., Odling, N.E., Davy, P., Main, I., Cowie, P., Berkowitz, B.: Scaling of fracture systems in geological media. Rev. Geophys. **39**, 347–383 (2001)

[CaEtAl94] Cairns, D.S., Ilcewicz, L.B., Walker, T., Minguet, P.J.: Fracture scaling parameters of inhomogeneous microstructure in composite structures. J. Compos. Mater. **28**, 1598–1615 (1994)

[CaCh95] Carpinteri, A., Chiaia, B.: Multifractal nature of concrete fracture surfaces and size effects on nominal fracture energy. Mater. Struct. **28**, 435–443 (1995)

[CaChCo03] Carpinteri, A., Chiaia, B., Cornetti, P.: On the mechanics of quasi-brittle materials with a fractal microstructure. Eng. Fract. Mech. **70**, 2321–2349 (2003)

[DaEtAl06] Davy, P., Darcel, C., Bour, O., Munier, R., de Dreuzy, J.R.: Reconstructing the 3D fracture distribution model from core—10cm—to lineament—10km—scales. Geophys. Res. Abstr. **8**, 07751 (2006)

[Fa97] Falconer, K.J.: Techniques in Fractal Geometry. Wiley, New York (1997)

[GhDa93] Ghosh, A., Daemen, J.J.H.: Fractal characteristics of rock discontinuities. Eng. Geol. **34**, 1–9 (1993)

[GiEtAl93] Gillespie, P.A., Howard, C.B., Walsh, J.J., Watterson, J.: Measurement and characterisation of spatial distribution of fractures. Tectonophysics **226**, 113–141 (1993)

[GoMuMa98] Gonzato, G., Mulargia, F., Marzocchi, W.: Practical application of fractal analysis: problems and solutions. Geophys. J. Int. **132**, 275–282 (1998)

[HaFl98] Halíř, R., Flusser, J.: Numerically stable direct least squares fitting of ellipses, http://autotrace.sourceforge.net/WSCG98.pdf (1998)

[Ha85] Hancock, P.L.: Brittle microtectonics, principles and practice. J. Struct. Geol. **7**, 437–457 (1985)

[Hi89] Hirata, T.: Fractal dimension of fault systems in Japan: fractal structure in rock fracture geometry at various scales. Pure Appl. Geophys. **131**, 157–170 (1989)

[HuPr79] Hudson, J.A., Priest, S.D.: Discontinuities and rock mass geometry. Int. J. Rock Mech. Min. Sci. Geomech. Abstr. **16**, 339–362 (1979)

[KuUmPa97] Kulatilake, P.H.S.W., Um, J., Pan, G.: Requirements for accurate estimation of fractal parameters for self-affine roughness scaling method. Rock Mech. Rock Eng. **30**, 181–206 (1997)

[LaEtAl02] Laubach, S.E., Reed, R.M., Gale, J.F.W., Ortega, O.J., Doherty, E.H.: Fracture characterization based on microfracture surrogates, Pottsville Sandstone, Black Warrior Basin, Alabama. Gulf Coast Assoc. Geol. Soc. Trans. **52**, 585–596 (2002)

[LiBZ05] Libicki, E., Ben-Zion, Y.: Stochastic branching models of fault surfaces and estimated fractal dimensions. Pure Appl. Geophys. **162**, 1077–1111 (2005)

[MoBoVa02] Morel, S., Bouchaud, E., Valentin, G.: Size effect in fracture: roughening of crack surfaces and asymptotic analysis. Phys. Rev. B **65**, 104101 (2002)

[NSEtAl05] Nieto-Samaniego, A.F., Alaniz-Alvarez, S.A., Tolson, G., Oleschko, K., Korvin, G., Xu, S.S., Pérez-Venzor, A.: Spatial distribution, scaling and self-similar behavior of fracture arrays in the Los Planes Fault, Baja California Sur, Mexico. Pure Appl. Geophys. **162**, 805–826 (2005)

[OdEtAl99] Odling, N.E., Gillespie, P., Bourgine, B., Castaing, C., Chilés, J.P., Christensen, N.P., Fillion, E., Genter, A., Olsen, C., Thrane, L., Trice, R., Aarseth, E., Walsh, A.A., Watterson, J.: Variations in fracture system geometry and their implications for fluid flow in fractured hydrocarbon reservoir. Petrol. Geosci. **5**, 373–384 (1999)

[OrMaLa06] Ortega, O.J., Marrett, R.A., Laubach, S.E.: A scale-independent approach to fracture intensity and average spacing measurement. AAPG Bull. **90**, 193–208 (2006)

[Pi56] Pincus, H.J.: Some vector and arithmetic operations on two-dimensional orientation variates, with applications to geological data. J. Geol. **64**, 533–557 (1956)

[PrVM03] Prado, E.P., Van Mier, J.G.M.: Effect of particle structure on mode I fracture process in concrete. Eng. Fract. Mech. **70**, 1793–1807 (2003)

[PuEtAl01] Putot, C., Chastanet, J., Cacas, M.C., Daniel, J.M.: Fractography in sedimentary rocks: tension joint sets and fracture swarms. Rev. Institut Français du Pétrole **56**, 431–449 (2001)

[RaHu87] Ramsay, J.G., Huber, M.I.: The Techniques of Modern Structural Geology. Academic, Oxford (1987)

[St93] Strieder, A.J.: Deformação e Metamorfismo na Região de Santa Cruz de Goiás. Correlação Tectono-Estratigráfica e Evolução Tectónica Regional. Doctoral Dissertation, Institute of Geosciences-UNB, Brasília (DF), Brazil (1993)

[StSu99] Strieder, A.J., Suita, M.T.F.: Neoproterozoic geotectonic evolution of Tocantins Structural Province, Central Brazil. J. Geodyn. **28**, 267–289 (1999)

[TeEtAl05] Telles, I.A., Vargas, E.A. Jr., Lira, W.W.M., Martha, L.F.: Uma Ferramenta Computacional para a Geração de Sistemas de Fraturas em Meios Rochosos, http://www.tecgraf.pucrio.br/publications/artigo_2005_ferramenta_computacional_geracao_sistemas_fraturas.pdf (2005)

[Tu97] Turcotte, D.L.: Fractals and Chaos in Geology and Geophysics. Cambridge University Press, Cambridge (1997)

[VeEtAl90] Velde, B., Dubois, J., Touchard, G., Badri, A.: Fractal analysis of fractures in rocks: the Cantor's Dust method. Tectonophysics **179**, 345–352 (1990)

[VeEtAl91] Velde, B., Dubois, J., Moore, D., Touchard, G.: Fractal patterns of fractures in granites. Earth Planet. Sci. Lett. **104**, 25–35 (1991)

[VoKr04] Vollanda, S., Kruhl, J.H.: Anisotropy quantification: the application of fractal geometry methods on tectonic fracture patterns of a Hercynian fault zone in NW Sardinia. J. Struct. Geol. **26**, 1499–1510 (2004)